Correlation between Mn and Ru valence states and magnetic phases in $SrMn_{1-x}Ru_xO_3$

D. H. Kim,[1] Eunsook Lee,[1] Hyun Woo Kim,[1] S. Kolesnik,[2] B. Dabrowski,[2] Chang-Jong Kang,[3] Minjae Kim,[3] B. I. Min,[3] Han-Koo Lee,[4] J.-Y. Kim,[4] and J.-S. Kang[1,*]

[1]*Department of Physics, The Catholic University of Korea, Bucheon 420-743, Korea*
[2]*Department of Physics, Northern Illinois University, DeKalb, Illinois 60115, USA*
[3]*Department of Physics, POSTECH, Pohang 790-784, Korea*
[4]*Pohang Accelerator Laboratory (PAL), POSTECH, Pohang 790-784, Korea*

(Received 3 August 2014; revised manuscript received 17 January 2015; published 17 February 2015)

The electronic structures of $SrMn_{1-x}Ru_xO_3$ ($0 \leqslant x \leqslant 1$) have been investigated by employing soft x-ray absorption spectroscopy (XAS) and soft x-ray magnetic circular dichroism (XMCD). Both Mn and Ru ions are nearly tetravalent (Mn^{4+}, Ru^{4+}) for the end members of $x = 0$ ($SrMnO_3$) and $x = 1$ ($SrRuO_3$). In the Ru-dilute concentration ($x \leqslant\sim 0.2$), Ru ions are pentavalent (Ru^{5+}), which transform neighboring Mn ions into the trivalent Mn^{3+} states via electron charge transfer. In the intermediate substitution regime, Mn and Ru ions are in the inhomogeneously mixed-valent states ($Mn^3 - Mn^{4+}$ and $Ru^4 - Ru^{5+}$). Finite Mn $2p$ XMCD signals are observed for $x > 0$, in agreement with the ferromagnetic, spin-glass, cluster-glass ground states depending on x. The unoccupied Mn $3d$ and Ru $4d$ states, determined from the measured O $1s$ XAS spectra and the calculated density of states, support these findings.

DOI: 10.1103/PhysRevB.91.075113 PACS number(s): 78.70.Dm, 78.20.Ls, 75.47.Lx, 71.28.+d

I. INTRODUCTION

$SrRuO_3$ is a unique ferromagnetic (FM) metallic oxide among $4d$ transition-metal (TM) perovskite oxides with a Curie temperature T_C of $\sim$ 160 K [1,2]. The noninteger value of the measured saturation magnetic moment of 1.6 μB/Ru in $SrRuO_3$ was considered to reflect the itinerant ferromagnetism [3] explained by the Stoner theory [4]. But this idea has not been confirmed fully by experiment. The substitution of $3d$ TM ions for Ru ions causes many intriguing properties, such as metal-insulator (MI) transition, FM-paramagnetic (PM) transition, FM-antiferromagnetic (AFM) transition, and enhanced magnetoresistance [5–12]. Mn-doped $SrRu_{1-y}Mn_yO_3$ exhibits the diverse magnetic states and interesting physical phenomena, such as FM, spin-glass (SG) and/or cluster-glass (CG), AFM, and mixed-valent behavior [5–7,10–12]. $SrMnO_3$ ($y = 1$) is a G-type AFM insulator with the Néel temperature T_N of $\sim$ 233 K [12]. The study of $SrRu_{1-y}Mn_yO_3$ ($0 \leqslant y < 0.6$) single crystals [7] has shown that, with increasing y, the Mn substitution drives the system from the itinerant FM state at $y = 0$ ($SrRuO_3$) through a quantum critical point (QCP) at $y = 0.39$ to the AFM insulating state. In contrast, the contradictory findings [6] and a more complex phase diagram [11,12] were reported for polycrystalline samples of $SrRu_{1-y}Mn_yO_3$.

The investigation of the electronic structures of $SrRu_{1-y}Mn_yO_3$ is very important to resolve these controversial issues because the magnetic ground states are determined by their electronic structures. In $SrRu_{1-y}Mn_yO_3$, electrons are considered to transfer from Ru^{4+} to Mn^{4+} ions. If this scenario is correct, then the valence states of Mn and Ru ions are expected to change via charge transfer to convert Mn^{4+} ($3d^3$) into Mn^{3+} ($3d^4$) and Ru^{4+} ($4d^4$) into Ru^{5+} ($4d^3$). This conceptual model was supported partially by the Ru and Mn L ($2p$)-edge x-ray absorption spectroscopy (XAS) experiment for the Ru-rich regime [6] and by the Mn NMR experiment for $SrRu_{0.9}Mn_{0.1}O_3$ [10]. But, this scenario has not been confirmed experimentally for the whole substitution range. Therefore, a systematic and careful study is required for the electronic structures of $SrRu_{1-y}Mn_yO_3$. Despite quite extensive studies on $SrRuO_3$ [6,7,13–17], however, only a few works have been reported for the electronic structures of $SrRu_{1-y}Mn_yO_3$ so far [6,11,17]. Sahu *et al.* [6] performed Mn $2p$ and Ru $2p$ XAS experiment on $SrRu_{1-y}Mn_yO_3$ to find the tendency of the charge transfer from Ru^{4+} to Mn^{4+} ions. Zhang *et al.* [11] performed x-ray photoemission spectroscopy (XPS) experiment for the Mn $2p$ and Ru $3d$ core levels of $SrRu_{1-y}Mn_yO_3$ to suggest the mixed-valence nature of Mn^{3+}/Mn^{4+} and Ru^{4+}/Ru^{5+} redox pairs. Horiba *et al.* [17] performed Mn $2p$ and Ru $2p$ XAS as well as valence-band photoemission spectroscopy (PES) experiment on $SrRu_{1-y}Mn_yO_3$ by using Mn $2p$–$3d$ resonance. They extracted the Mn $3d$ partial density of states (PDOS) near the Fermi level (E_F) and concluded that the charge transfer occurred from the itinerant Ru $4d$ t_{2g} bands to the localized Mn $3d$ e_g orbitals.

In this paper, we have investigated the electronic and magnetic structures of $SrMn_{1-x}Ru_xO_3$ by employing Mn $2p$ and Ru $3p$ XAS and x-ray magnetic circular dichroism (XMCD), for which the soft x-ray synchrotron radiation was used as the excitation photon source. XAS is known to be a powerful experimental tool for studying electronic structures of solids [18–20], which can determine the valence and spin states of TM ions. XMCD is a good experimental tool for determining the spin configurations of TM ions and the spin and orbital components of the element-specific local magnetic moments in solids [21,22]. We have also performed the O $1s$ XAS measurements on $SrMn_{1-x}Ru_xO_3$ to extract the unoccupied PDOSs, which are compared with the calculated PDOSs of $SrMn_{0.5}Ru_{0.5}O_3$.

II. EXPERIMENTAL AND COMPUTATIONAL DETAILS

Polycrystalline $SrMn_{1-x}Ru_xO_3$ perovskite samples are prepared using a two-step synthesis method, as described

*Corresponding author: kangjs@catholic.ac.kr

in Ref. [12]. X-ray diffraction (XRD) measurements show that these samples have the single-phase perovskite structure. XAS and XMCD experiments were performed at the 2A elliptically polarized undulator (EPU) beamline of the Pohang Light Source (PLS). Samples were cleaned *in situ* by repeated scraping with a diamond file. The chamber pressure was better than 3×10^{-10} Torr. XAS and XMCD spectra were obtained by using the total electron yield mode, and XMCD spectra were obtained under the magnetic field of $H \sim 0.6$ T. The total resolution for XAS and XMCD was set at ~ 100 meV at $h\nu \sim 600$ eV. All the spectra were normalized to the incident photon flux.

We have obtained PDOSs of $SrMn_{0.5}Ru_{0.5}O_3$ by performing the density-functional theory (DFT) band calculations incorporating the Coulomb correlations (U) of Mn and Ru d electrons (DFT + U scheme). For the band calculation, we have employed the full-potential linearized augmented plane wave (FLAPW) band method implemented in the Wien2k package [23]. For the treatment of the exchange-correlation potential, the generalized gradient approximation (GGA) has been used.

III. RESULTS AND DISCUSSION

Figure 1(a) shows the Mn $2p$ (L-edge) XAS spectra of $SrMn_{1-x}Ru_xO_3$ for $0 \leqslant x \leqslant 0.8$, measured at $T = 80$ K. As reference materials, the spectra of a formally tetravalent MnO_2 (Mn^{4+}: $3d^3$) [24–26] and a formally trivalent Mn_2O_3 (Mn^{3+}: $3d^4$) [24] are also shown together. L_3 ($2p_{3/2}$) and L_2 ($2p_{1/2}$) represent the spin-orbit-split peaks due to the spin-orbit coupling of the $2p$ core hole. It is well known that the Mn $2p$ XAS peak positions shift toward higher energies as the Mn valency increases [25]. It is clearly seen that the main peak (peak B) at high Ru concentrations ($x \geqslant 0.5$) is located at a lower $h\nu$ than that (peak A) at low Ru concentrations ($x \leqslant 0.2$). The peak positions for $x \leqslant 0.2$ are close to those of tetravalent MnO_2 while those for $x \geqslant 0.5$ are very close to those of trivalent Mn_2O_3, indicating that v(Mn)≈ 4 for $x \leqslant 0.2$ and v(Mn) ≈ 3 for $x \geqslant 0.5$. This trend indicates that the valence states of Mn ions change with x in $SrMn_{1-x}Ru_xO_3$ [6,17–19,27,28].

A more detailed comparison is made in Fig. 1(b), showing that the peak position stays the same between $0 \leqslant x \leqslant 0.2$, shifts abruptly to a lower energy from $x = 0.2$ to $x = 0.5$, and then stays the same between $0.5 \leqslant x \leqslant 0.8$. In addition, the peak positions for $x \leqslant 0.2$ agree very well with that of MnO_2 while those for $x \geqslant 0.5$ agree very well with that of Mn_2O_3. The less pronounced pre-edge peak ($h\nu \approx 640$ eV) in $SrMnO_3$, as compared to MnO_2, is expected to reflect the stronger covalent bonding character in $SrMnO_3$ than in MnO_2 [29], which results in the broader multiplet structures in $SrMnO_3$ than in MnO_2.

In Fig. 1(c), we have compared the XAS spectrum of $x = 0.8$ with those of Mn_2O_3 and the weighted sum of those of Mn_2O_3 (Mn^{3+}) and MnO_2 (Mn^{4+}) with Mn^{3+}: Mn^{4+}=80%: 20%. Both comparisons show reasonably good agreement, with a slightly better agreement with the weighted sum than with Mn_2O_3. These two comparisons at the top provide evidence that the average Mn valency v(Mn) for $x \geqslant 0.5$ to be v(Mn) $\approx 3 - 3.2$ within the experimental uncertainty. At the bottom of Fig. 1(c), we have compared the XAS spectrum of $x = 0$ ($SrMnO_3$) with that of MnO_2, which shows good agreement in the peak positions except for the weaker pre-edge feature in $SrMnO_3$ than in MnO_2. Hence Fig. 1

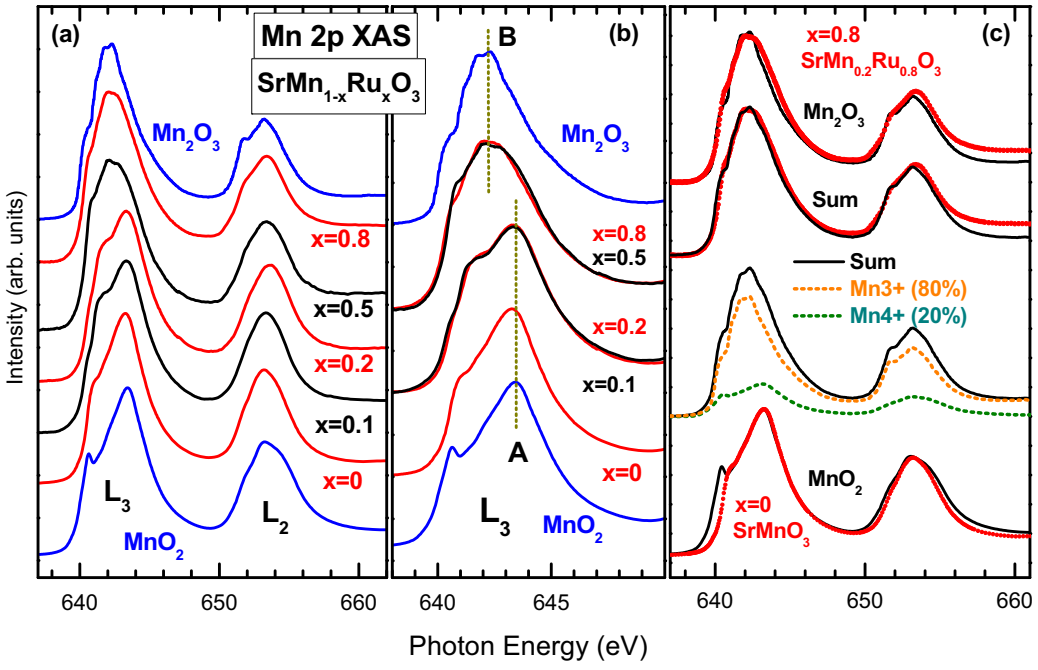

FIG. 1. (Color online) (a) Mn $2p$ XAS spectra of $SrMn_{1-x}Ru_xO_3$ ($0 \leqslant x \leqslant 0.8$) in stack, obtained at $T = 80$ K. (b) Similarly as in (a), where some of them are superposed to each other. (c) Comparison of the Mn $2p$ XAS spectrum of $x = 0$ ($SrMnO_3$) with that of MnO_2 (Mn^{4+}) (bottom). The Mn $2p$ XAS spectrum of $x = 0.8$ is compared with that of Mn_2O_3 (Mn^{3+}) as well as with the weighted sum of Mn_2O_3 (Mn^{3+}) and MnO_2 (Mn^{4+}).

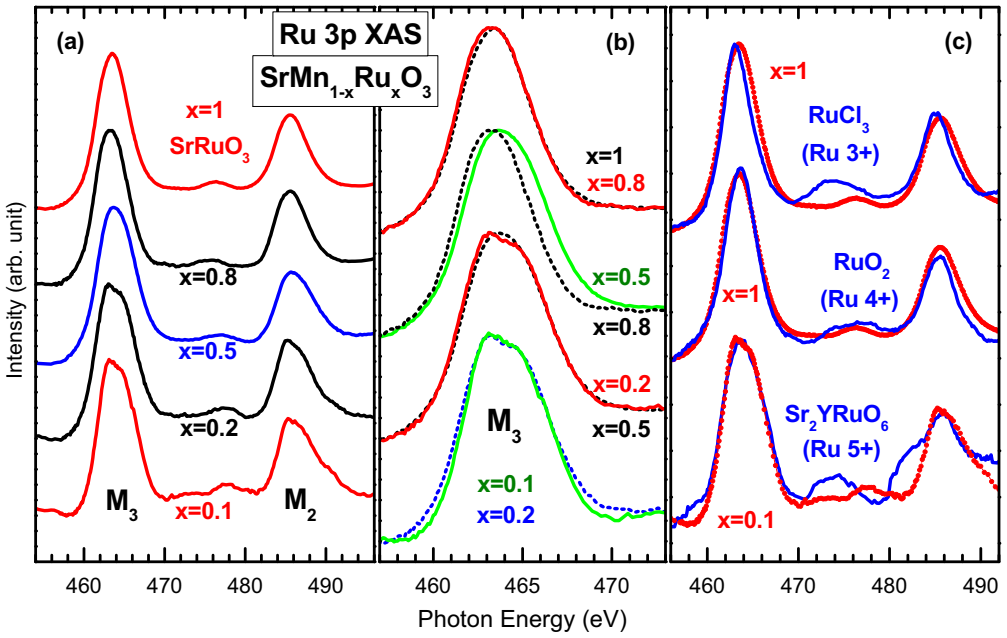

FIG. 2. (Color online) (a) Ru $3p$ XAS spectra of $SrMn_{1-x}Ru_xO_3$ ($0 \leqslant x \leqslant 0.8$) in stack, obtained at $T = 80$ K. (b) Similarly as in (a), where two nearby x data are superposed to each other. (c) Comparison of the Ru $3p$ XAS spectra of $x = 1$ ($SrRuO_3$) and $x = 0.1$ ($SrMn_{0.9}Ru_{0.1}O_3$) with those of reference materials, such as $RuCl_3$ (Ru^{3+}), RuO_2 (Ru^{4+}) and Sr_2YRuO_6 (Ru^{5+}).

provides evidence that, in $SrMn_{1-x}Ru_xO_3$, v(Mn) decreases from $v(\mathrm{Mn}) \approx 4$ in the Ru-dilute regime ($x \leqslant 0.2$) to $v(\mathrm{Mn}) \approx 3 - 3.2$ in the Ru-rich regime ($x \geqslant 0.5$). Namely, Mn ions are inhomogeneously mixed-valent for $x > 0$ in $SrMn_{1-x}Ru_xO_3$. This finding implies that most Mn ions around Ru ions are trivalent (Mn^{3+}).

The finding of the different valence states of Mn ions with x in $SrMn_{1-x}Ru_xO_3$ suggests that the valence states of Ru ions should also vary with x. In order to determine the valence states of Ru ions experimentally, we have measured the Ru $3p$ (M-edge) XAS spectra of $SrMn_{1-x}Ru_xO_3$. Figure 2 shows the Ru $3p$ XAS spectra of $SrMn_{1-x}Ru_xO_3$ for $0.1 \leqslant x \leqslant 1$, measured at $T = 80$ K. M_3 and M_2 denote the spin-orbit-split $3p_{3/2}$ (M_3) and $3p_{1/2}$ (M_2) peaks. The line shapes of the Ru $3p$ XAS spectra are less structured than those of the Mn $2p$ XAS spectra, reflecting the much weaker Coulomb interaction between Ru $4d$ electrons than that between Mn $3d$ electrons. In other words, Ru $4d$ electrons have the more itinerant character than Mn $3d$ electrons.

Figures 2(a) and 2(b) show that both the peak positions and the line shapes of the Ru $3p$ XAS spectra are almost identical from $x = 1$ to $x = 0.8$, indicating that v(Ru) is almost the same for $x = 1$ and $x = 0.8$. Then, as x decreases from $x = 0.8$ to $x = 0.5$, the peaks become broader and shift toward the higher energies slightly, and stay unchanged with decreasing x from $x = 0.5$ to $x = 0.1$. This trend indicates the emergence of an extra peak at the high-energy side of the main peak for $x \leqslant 0.5$, probably due to the Ru^{5+} valence states. This assignment is confirmed by the comparison to the reference materials having the different Ru valencies, such as $RuCl_3$, RuO_2, and Sr_2YRuO_6 for Ru^{3+}, Ru^{4+}, and Ru^{5+}, respectively, as shown in Fig. 2(c). As in the $2p$ XAS of $3d$ TM ions, the Ru $3p$ XAS peaks shift to the higher $h\nu$'s as the Ru valency increases. Indeed, both the peak positions and the peak widths of $x = 1$ ($SrRuO_3$) and $x = 0.1$ ($SrMn_{0.9}Ru_{0.1}O_3$) match very well with those of RuO_2 (Ru^{4+}) and Sr_2YRuO_6 (Ru^{5+}), respectively [see Fig. 2(c)]. Hence Fig. 2 reveals that the valence states of Ru ions are nearly tetravalent (Ru^{4+}) for $x \geqslant 0.8$ and become nearly pentavalent ($\approx Ru^{5+}$) for $x \leqslant 0.5$.

The findings of Figs. 1 and 2 are summarized in Fig. 3, where the measured values of v(Mn) and v(Ru) are plotted as blue and red dots. The dotted lines represent the estimated values of v(Mn) and v(Ru) by assuming the charge transfer between Mn and Ru. From Figs. 1 and 2, we have found $v(\mathrm{Ru}) \approx 5$ for $x \leqslant 0.5$ and $v(\mathrm{Mn}) \approx 3$ for $x \geqslant 0.5$. So, for

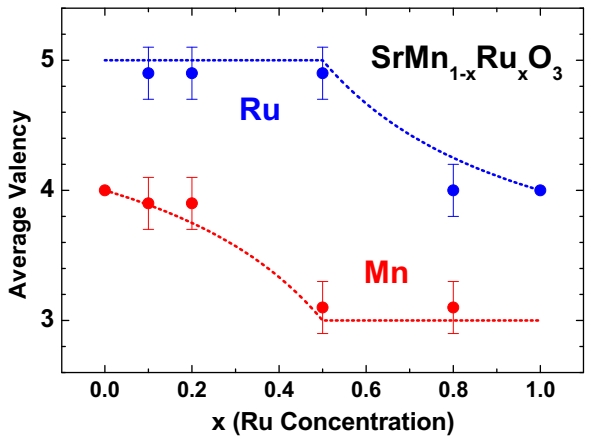

FIG. 3. (Color online) Plots of the average valencies of Mn and Ru ions in $SrMn_{1-x}Ru_xO_3$ for $0 \leqslant x \leqslant 1$. Dots represent the experimental values, determined from the measured Mn $2p$ and Ru $3p$ XAS spectra. The dotted lines represent the values for the valence states of Mn (red) and Ru (blue), expected for the charge transfer between Mn and Ru.

$x \leqslant 0.5$, v(Mn) is estimated by assuming v(Ru) $= 5$, and for $x \geqslant 0.5$, v(Ru) is estimated by assuming v(Mn) $= 3$. For both cases, the charge transfer from Ru to Mn has been assumed. In the Ru-dilute limit ($x \leqslant\sim 0.2$), Ru ions become pentavalent (Ru^{5+}), which then transform neighboring Mn^{4+} ions to the Mn^{3+} ions via the electron transfer from Ru^{4+} to Mn^{4+}. But, the measured Mn $2p$ XAS spectrum in the Ru-dilute limit appears to be nearly tetravalent (Mn^{4+}) with only a weak hint of the Mn^{3+} component because of the large contribution from Mn^{4+}. Similarly, in the Mn-dilute limit, most of Mn ions are trivalent (Mn^{3+}) and neighboring Ru ions will become locally pentavalent ($Ru^{5}+$). But the measured Ru $3p$ XAS spectrum reveals only a weak hint of the Ru^{5+} component. In the intermediate regime, Mn and Ru ions become inhomogeneously mixed-valent, having the configurations of $Mn^{3} - Mn^{4+}$ ($x < 0.5$) and $Ru^{4} - Ru^{5+}$ ($x > 0.5$), respectively. This figure shows that the average valencies of Mn and Ru ions determined from the XAS data agree well with the expected charge transfer scenario from Ru to Mn within the experimental uncertainty.

It should be pointed out that there are some discrepancies between the present work and that by Horiba *et al.* [17]. Namely, the line shape of our Mn $2p$ XAS spectrum for $x = 0.2$ is different from that in Ref. [17] slightly. Further, the trends in the peak shift of Mn $2p$ XAS and Ru $3p$ XAS are different from those of Mn $2p$ XAS and Ru $2p$ XAS in Ref. [17]. At the moment, we do not know the origin of such differences between our data and those in Ref. [17]. We note that the data in Ref. [17] were obtained from fracture whereas our data were obtained from the repeated scraping *in situ*. All of our samples are stoichiometric and are characterized very well, as described in Ref. [12], and we did very careful measurement. We scraped the samples many times and checked the reproducibility of all the data. Note that our Mn $2p$ XAS data for $x = 0$, $x = 0.1$, and $x = 0.2$ are very similar to one another, which seems to support the validity of our data for $x = 0$, 0.1, 0.2. One possibility could be the impurity MnO_2 cluster, which was in the grain boundaries of a polycrystalline sample and then exposed in some fractures. In order to resolve this issue, however, a very careful measurement for the well-characterized single crystalline samples of $SrMn_{1-x}Ru_xO_3$ would be desirable.

Figures 4(a) and 4(b) show Mn $2p$ and Ru $3p$ XMCD spectra of $SrMn_{1-x}Ru_xO_3$, measured at $T = 80$ K, respectively. The Ru $3p$ XMCD signals are finite only for $x = 1$ ($SrRuO_3$), and negligible for $x \leqslant 0.8$. This trend is consistent with the FM ground state for $x = 1$ [see Fig. 5(c)]. On the other hand, the finite Mn $2p$ XMCD signals are observed for $x > 0$ in $SrMn_{1-x}Ru_xO_3$ with the maximum intensity for $x = 0.5$. According to the *bulk* phase diagram of $SrMn_{1-x}Ru_xO_3$ in Fig. 5(c), $x = 0.5$ is on the border of the AFM and paramagnetic (PM)/spin glass (SG) state while $x = 0.8$ is in the PM state at $T = 80$ K. Hence the observed finite Mn $2p$ XMCD signals seem to reflect the existence of the local short-range magnetic orderings in $x = 0.5$ and $x = 0.8$ due to the presence of the applied external magnetic field. The consistency between the measured XMCD signals and the magnetic phase diagram of $SrMn_{1-x}Ru_xO_3$ is shown more clearly in Fig. 5.

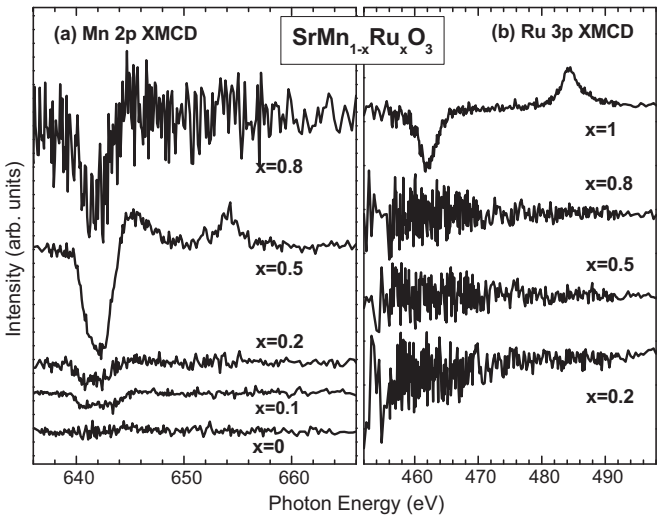

FIG. 4. (a) Mn $2p$ XMCD spectra and (b) Ru $3p$ XMCD spectra of $SrMn_{1-x}Ru_xO_3$ ($0 \leqslant x \leqslant 1$), obtained at $T = 80$ K.

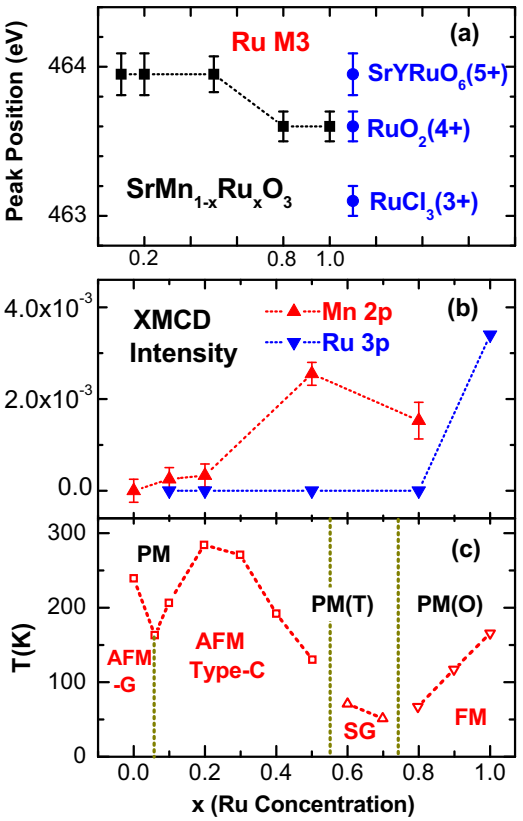

FIG. 5. (Color online) (a) Plots of the center positions of the Ru M_3 ($3p_{3/2}$) peaks of $SrMn_{1-x}Ru_xO_3$, together with those of reference materials, such as $RuCl_3$ (Ru^{3+}), RuO_2 (Ru^{4+}), and Sr_2YRuO_6 (Ru^{5+}). (b) Peak-to-peak intensity plots of the Mn $2p$ and Ru $3p$ XMCD signals of $SrMn_{1-x}Ru_xO_3$, as a function of x. These are normalized to the corresponding XAS signals. (c) Magnetic phase diagram of $SrMn_{1-x}Ru_xO_3$ as a function of x [from Ref. [12]]. T and O denote the tetragonal and orthorhombic structures, respectively.

Figure 5(a) plots the center positions of the Ru M_3 ($3p_{3/2}$) peaks of $SrMn_{1-x}Ru_xO_3$ versus x, together with those of reference materials, such as $RuCl_3$ (Ru^{3+}), RuO_2 (Ru^{4+}), and Sr_2YRuO_6 (Ru^{5+}). This plot reveals that, in the Ru-dilute concentration ($x \leqslant 0.2$), the Ru M_3 peak position is very similar to that of Sr_2YRuO_6 (Ru^{5+}) while it becomes essentially the same as that of RuO_2 (Ru^{4+}) in the Ru-rich concentration ($x \geqslant 0.8$). The valence states of Ru ions are nearly tetravalent (Ru^{4+}) for $x = 1$ ($SrRuO_3$) and they become $Ru^{4+} - Ru^{5+}$ mixed-valent as Ru ions are substituted by Mn ions. In the Ru-dilute limit, most of Ru ions are pentavalent (Ru^{5+}).

Figures 5(b) and 5(c) show the peak-to-peak intensity plots of the Mn $2p$ and Ru $3p$ XMCD signals and the *bulk* magnetic phase diagram, respectively, of $SrMn_{1-x}Ru_xO_3$ as a function of x. The former intensities were determined from Fig. 4 and the latter phase diagram was made based on the results of Ref. [12]. This figure reveals that the trends observed in Mn $2p$ and Ru $3p$ XMCD are in agreement with the corresponding magnetic states of $SrMn_{1-x}Ru_xO_3$, as explained below. The finite Ru $3p$ XMCD signals in $x = 1$ ($SrRuO_3$) in Fig. 5(b) supports its FM ground state, shown in Fig. 5(c). The finite Mn $2p$ XMCD signals for $x = 0.5$ and $x = 0.8$ in Fig. 5(b) also agree with the magnetic phase diagram of $SrMn_{1-x}Ru_xO_3$ in Fig. 5(c), considering the possible local short-range magnetic orderings in the SG and PM states due to the applied external magnetic field.

In order to check the unoccupied electronic states of Mn and Ru ions, we compare the O $1s$ XAS spectra of $SrMn_{1-x}Ru_xO_3$ in Fig. 6. The O $1s$ XAS spectra of TM oxides represent the unoccupied TM $3d$ and $4s/4p$ states, as well as the other conduction-band states via the hybridization with the unoccupied O $2p$ states [30]. Therefore, we assign the peaks in O $1s$ XAS similarly as in other TM oxides [31]. Our O $1s$ XAS spectrum of *bulk* $SrRuO_3$ exhibits sharper peaks than that of $SrRuO_3$ film [14] with similar overall features. The lowest-energy peaks in $SrMn_{1-x}Ru_xO_3$ are due to the unoccupied Mn $3d$ states or the Ru $4d$ states. As labeled in Fig. 6(a), the peaks at $h\nu \sim 535$ eV are identified as the unoccupied Sr $4d$ states [29], and the peaks at $h\nu \sim 540 - 545$ eV are assigned to the unoccupied Mn $4sp$ and Ru $5sp$ states.

We have found that Mn ions are tetravalent in $SrMnO_3$ (see Fig. 1) having the Mn^{4+} ($3d^3$: t_{2g}^3 ↑) configuration. Hence, the lowest-energy peak in the O $1s$ XAS of $SrMnO_3$ ($x = 0$) corresponds to the unoccupied Mn e_g ↑ band, superposed with the unoccupied Mn t_{2g} ↓ states [see Fig. 6(b)]. This assignment agrees with that of Ref. [32], but different from that of Ref. [33] slightly. On the other hand, for $SrRuO_3$ ($x = 1$) having Ru^{4+} ions ($4d^4$: t_{2g}^3 ↑ t_{2g}^1 ↓), E_F lies in the partially filled t_{2g} ↓ bands, resulting in the metallic ground state. Therefore the lowest-energy peak in the O $1s$ XAS of $SrRuO_3$ ($x = 1$) corresponds to the partially unoccupied Ru t_{2g} band. The AFM ground state for $x = 0.5$ [see Fig. 5(c)] has the occupied configuration of Mn^{3+} ($3d^4$: t_{2g}^3 ↑ e_g^1 ↑) and Ru^{5+} ($4d^3$: t_{2g}^3 ↓), and so the low-energy unoccupied states are Ru t_{2g} ↑, Mn e_g ↑, and Mn t_{2g} ↓ states. According to these O $1s$ XAS spectra, the crystal field energy ($10Dq$) is $10Dq \sim 2$ eV for Mn $3d$ orbitals and $10Dq \sim 3$ eV for Ru $4d$ orbitals in $SrMn_{1-x}Ru_xO_3$.

In order to analyze the XMCD and O $1s$ XAS spectra of $SrMn_{1-x}Ru_xO_3$ microscopically, we have investigated the electronic structures of Sr_2MnRuO_6 theoretically. In Fig. 7 are presented the calculated PDOSs, obtained for the c-type AFM phase of Sr_2MnRuO_6 in the orthorhombic structure [34] by employing the DFT + U band calculation. In fact, the electronic structures of Sr_2MnRuO_6 were calculated before [34,35]. But, the previous band structure calculations [34,35] did not take

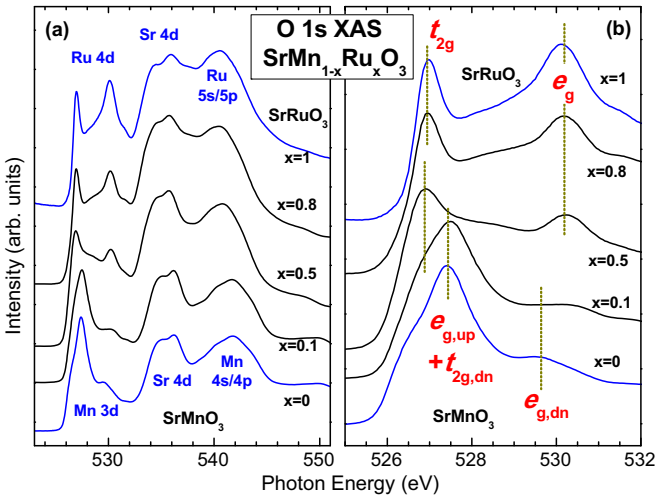

FIG. 6. (Color online) (a) O $1s$ XAS spectra of $SrMn_{1-x}Ru_xO_3$ ($0 \leqslant x \leqslant 1$), obtained at $T = 300$ K. (b) Enlarged O $1s$ XAS spectra of (a).

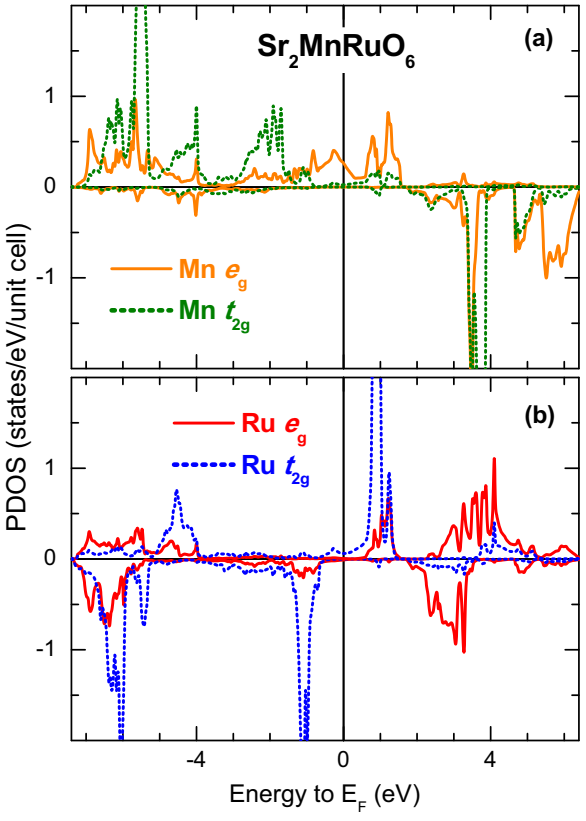

FIG. 7. (Color online) The calculated PDOSs of Sr_2MnRuO_6 obtained in the DFT + U scheme, where $U = 5$ eV and $U = 3$ eV were adopted for Mn $3d$ and Ru $4d$ electrons, respectively.

into account the correct crystal or magnetic structure properly. Moreover, the effects of U of the Mn and Ru d electrons were not included either. In the c-type AFM structure, the spin directions of Mn and Ru ions are parallel along the c direction but antiparallel in the ab plane. Figure 7 shows the following features. (i) The Mn $3d$ band has the high-spin state, while the Ru $4d$ band has the low-spin state. (ii) The Ru t_{2g} spin-up and spin-down bands are rather sharp and separated far apart, and so the unoccupied Ru t_{2g} band is located away from E_F in contrast to metallic $SrRuO_3$. (iii) The Mn e_g spin-up band is widely spread over E_F so as to produce a shoulder in the low-$h\nu$ side of the unoccupied Mn $3d$ band. Therefore, the overall features of the unoccupied PDOSs in Fig. 7 are very consistent with those of the O $1s$ XAS spectrum for $x = 0.5$ in Fig. 6.

IV. CONCLUSION

The electronic structures of $SrMn_{1-x}Ru_xO_3$ ($0 \leqslant x \leqslant 1$) have been investigated by employing XAS and XMCD at the Mn $2p$ and Ru $3p$ absorption edges and the DFT + U band method. The measured Mn $2p$ XAS spectra of $SrMn_{1-x}Ru_xO_3$ show the systematic changes, indicating that both Mn and Ru ions are nearly tetravalent (Mn^{4+}, Ru^{4+}) for the end members of $x = 0$ ($SrMnO_3$) and $x = 1$ ($SrRuO_3$). In the intermediate substitution regime, Mn and Ru ions become inhomogeneously mixed-valent, having the $Mn^3 - Mn^{4+}$ ($x < 0.5$) and $Ru^4 - Ru^{5+}$ ($x > 0.5$) configurations, respectively. In the Ru-dilute concentration ($x \leqslant\sim 0.2$), Ru^{4+} ions become Ru^{5+}, which then transform the neighboring Mn^{4+} ions to Mn^{3+} ions via the expected electron charge transfer from Ru^{4+} to Mn^{4+}. Finite Mn $2p$ XMCD signals are observed for $x > 0$ in $SrMn_{1-x}Ru_xO_3$ with the maximum intensity for $x = 0.5$. On the other hand, except for $x = 1$ ($SrRuO_3$), the Ru $3p$ XMCD signals are almost negligible for $x \leqslant 0.8$. This trend is consistent with the FM ground state for $x \geqslant 0.8$ and the CG and/or SG ground states For $0.5 \leqslant x \leqslant 0.7$. The unoccupied Mn $3d$ and Ru $4d$ states have been determined from the measured O $1s$ XAS spectra and the calculated PDOSs, which are found to support these findings. The calculated PDOSs for the ordered $SrMn_{0.5}Ru_{0.5}O_3$, obtained in the DFT + U band method, show that the Mn $3d$ band has the high-spin state, while the Ru $4d$ band has the low-spin state.

ACKNOWLEDGMENTS

This work was supported by the National Research Foundation of Korea (NRF) under Contract Nos. 2011-0022444 and 2014R1A1A2056546, by the POSTECH BSRI grant, and by the Korea Institute of Science and Technology Information (KISTI) (Project No. KSC-2013-C3-010). Experiment at the PLS was supported by Ministry of Science, ICT and Future Planning (MSIP) and PAL, Korea. Work at NIU was supported by The Institute for Nanoscience, Engineering, and Technology - InSET. J.Y.K. acknowledges the support by the NRF (Grant No. 2012R1A2A2A02013936).

[1] A. Callanghan, C. W. Moller, and R. Ward, Inorg. Chem. **5**, 1572 (1966).
[2] J. M. Longo, P. M. Raccah, and J. B. Goodenough, J. Appl. Phys. **39**, 1327 (1968).
[3] G. Cao, S. McCall, M. Shepard, J. E. Crow, and R. P. Guertin, Phys. Rev. B **56**, 321 (1997).
[4] E. C. Stoner, Proc. Phys. Soc. A **165**, 372 (1938).
[5] A. Maignan, C. Martin, M. Hervieu, and B. Raveau, J. Appl. Phys. **91**, 4267 (2002).
[6] R. K. Sahu, Z. Hu, M. L. Rao, S. S. Manoharan, T. Schmidt, B. Richter, M. Knupfer, M. Golden, J. Fink, and C. M. Schneider, Phys. Rev. B **66**, 144415 (2002).
[7] G. Cao, S. Chikara, X. N. Lin, E. Elhami, V. Durairaj, and P. Schlottmann, Phys. Rev. B **71**, 035104 (2005).
[8] K. W. Kim, J. S. Lee, T. W. Noh, S. R. Lee, and K. Char, Phys. Rev. B **71**, 125104 (2005).
[9] A. J. Williams, A. Gillies, J. P. Attfield, G. Heymann, H. Huppertz, M. J. Martinez-Lope, and J. A. Alonso, Phys. Rev. B **73**, 104409 (2006).
[10] Z. H. Han, J. I. Budnick, W. A. Hines, B. Dabrowski, and T. Maxwell, Appl. Phys. Lett. **89**, 102501 (2006).
[11] Xiao-Yu Zhang, Yajie Chen, Zhen-Ya Li, Carmine Vittoria, and Vincent G. Harris, J. Phys. : Condens. Matter **19**, 266211 (2007).
[12] S. Kolesnik, B. Dabrowski, and O. Chmaissem, Phys. Rev. B **78**, 214425 (2008).
[13] K. Fujioka, J. Okamoto, T. Mizokawa, A. Fujimori, I. Hase, M. Abbate, H. J. Lin, C. T. Chen, Y. Takeda, and M. Takano, Phys. Rev. B **56**, 6380 (1997).
[14] J. Park, S.-J. Oh, J.-H. Park, D. M. Kim, and C.-B. Eom, Phys. Rev. B **69**, 085108 (2004).
[15] B. Dabrowski, S. Kolesnik, O. Chmaissem, T. Maxwell, M. Avdeev, P. W. Barnes, and J. D. Jorgensen, Phys. Rev. B **72**, 054428 (2005).
[16] J. Okamoto, T. Okane, Y. Saitoh, K. Terai, S.-I. Fujimori, Y. Muramatsu, K. Yoshii, K. Mamiya, T. Koide, A. Fujimori, Z. Fang, Y. Takeda, and M. Takano, Phys. Rev. B **76**, 184441 (2007).
[17] K. Horiba, H. Kawanaka, Y. Aiura, T. Saitoh, C. Satoh, Y. Kikuchi, M. Yokoyama, Y. Nishihara, R. Eguchi, Y. Senba, H. Ohashi, Y. Kitajima, and S. Shin, Phys. Rev. B **81**, 245127 (2010).
[18] F. M. F. de Groot, J. C. Fuggle, B. T. Thole, and G. A. Sawatzky, Phys. Rev. B **42**, 5459 (1990).
[19] G. van der Laan and I. W. Kirkman, J. Phys.: Condens. Matter **4**, 4189 (1992).
[20] S. C. Wi, J.-S. Kang, J. H. Kim, S.-B. Cho, B. J. Kim, S. Yoon, B. J. Suh, S. W. Han, K. H. Kim, K. J. Kim, B. S. Kim, H. J. Song, H. J. Shin, J. H. Shim, and B. I. Min, Appl. Phys. Lett. **84**, 4233 (2004).
[21] B. T. Thole, P. Carra, F. Sette, and G. van der Laan, Phys. Rev. Lett. **68**, 1943 (1992).
[22] C. T. Chen, Y. U. Idzerda, H.-J. Lin, N. V. Smith, G. Meigs, E. Chaban, G. H. Ho, E. Pellegrin, and F. Sette, Phys. Rev. Lett. **75**, 152 (1995).
[23] P. Blaha, K. Schwarz, G. Madsen, D. Kvasnicka, and J. Luitz, *WIEN2k, An Augmented Plane Wave+Local Orbitals Program*

for Calculating Crystal Properties, edited by K. Schwarz (Tech. Univ. Wien, Austria, 2001).

[24] P. Ghigna, A. Campana, A. Lascialfari, A. Caneschi, D. Gatteschi, A. Tagliaferri, and F. Borgatti, Phys. Rev. B **64**, 132413 (2001).

[25] C. Mitra, Z. Hu, P. Raychaudhuri, S. Wirth, S. I. Csiszar, H. H. Hsieh, H.-J. Lin, C. T. Chen, and L. H. Tjeng, Phys. Rev. B **67**, 092404 (2003).

[26] We have measured MnO_2 powder, which is the commercially available polycrystalline powder of the 99.99% purity. MnO_2 powder sample was mounted on the same sample holder as $SrMn_{1-x}Ru_xO_3$ samples and measured as is at room temperature.

[27] M. Abbate, F. M. F. de Groot, J. C. Fuggle, A. Fujimori, O. Strebel, F. Lopez, M. Domke, G. Kaindl, G. A. Sawatzky, M. Takano, Y. Takeda, H. Eisaki, and S. Uchida, Phys. Rev. B **46**, 4511 (1992).

[28] The peak positions and the spectral shapes of the $2p$ XAS spectra of transition-metal (TM) oxides reflect the $2p$ core-hole final-state multiplets, determined by the number of the occupied $3d$ electrons, to which the strong Coulomb interaction between $TM3d$ electrons and that between the $2p$ core hole and $3d$ electrons, the crystal field, and the hybridization interaction between the $TM3d$ electrons and the O $2p$ ligands also contribute.

[29] J.-S. Kang, H. J. Lee, G. Kim, D. H. Kim, B. Dabrowski, S. Kolesnik, Hangil Lee, J.-Y. Kim, and B. I. Min, Phys. Rev. B **78**, 054434 (2008).

[30] J.-S. Kang, S. W. Han, J.-G. Park, S. C. Wi, S. S. Lee, G. Kim, H. J. Song, H. J. Shin, W. Jo, and B. I. Min, Phys. Rev. B **71**, 092405 (2005).

[31] J. H. Hwang, D. H. Kim, J.-S. Kang, S. Kolesnik, O. Chmaissem, J. Mais, B. Dabrowski, J. Baik, H. J. Shin, Jieun Lee, Bongjae Kim, and B. I. Min, Phys. Rev. B **83**, 073103 (2011).

[32] D. H. Kim, H. J. Lee, B. Dabrowski, S. Kolesnik, Jieun Lee, Bongjae Kim, B. I. Min, and J.-S. Kang, Phys. Rev. B **81**, 073101 (2010).

[33] T. Saitoh, A. E. Bocquet, T. Mizokawa, H. Namatame, A. Fujimori, M. Abbate, Y. Takeda, and M. Takano, Phys. Rev. B **51**, 13942 (1995).

[34] P. M. Woodward, J. Goldberger, M. W. Stoltzfus, H. W. Eng, R. A. Ricciardo, P. N. Santhosh, P. Karen, and A. R. Moodenbaugh, J. Am. Ceram. Soc. **91**, 1796 (2008).

[35] B. Singh, S. S. Manoharan, R. K. Sahu, P. S. R. Krishnan, A. B. Shinde, and K. Jain, J. Appl. Phys. **101**, 09G518 (2007).